

Effective ALP-Photon Coupling in External Magnetic Fields

O. Semin*

*Institute for Theoretical Physics, Auf der Morgenstelle 14, University of Tübingen, Tübingen
72076, Germany*

May 9, 2025

Abstract

We present a complete calculation of the one-loop fermionic correction to the effective coupling between axion-like particles (ALPs) and photons within a constant, homogeneous magnetic field of arbitrary strength. This interaction, responsible for the Primakoff effect, is central to detecting axion-like particles in astrophysical settings and terrestrial experiments like helioscopes and haloscopes. Accurately predicting the interaction rate requires accounting for quantum corrections. Our work tackles this by employing magnetically enhanced fermion propagators derived using Schwinger's proper time method and a systematic Lorentz decomposition using the Ritus basis. We evaluate the triangle loop diagram exactly, avoiding approximations on field strength or particle kinematics.

1 Introduction

The Standard Model (SM) of particle physics, despite its remarkable success in describing fundamental particles and their interactions, falls short of describing the full picture. Among the most pressing is the nature of dark matter, which constitutes the vast majority of matter in the universe [1–3]. Its existence is inferred from overwhelming gravitational evidence, yet its composition remains uncertain, pointing towards physics Beyond the Standard Model (BSM) [4–7]. This gap in our understanding motivates a wide-ranging theoretical and experimental search for new particles.

Among the most promising BSM candidates are axions and axion-like particles (ALPs) [8]. The original QCD axion emerged as an elegant solution to the strong CP problem inherent in Quantum Chromodynamics (QCD), while ALPs arise more generally in various theoretical extensions of the SM, including string theory [9]. These light, pseudoscalar bosons are not only theoretically well-motivated but also serve as viable dark matter candidates. A

*ozan.semin@uni-tuebingen.de

key phenomenological feature of ALPs is their potential coupling to photons, often parameterized by the coupling constant $g_{a\gamma\gamma}$. This interaction opens a window for their detection, as it mediates the conversion of ALPs into photons (and vice versa) in the presence of external electromagnetic fields, a phenomenon known as the Primakoff effect [10].

The study of ALP-photon conversion has been a very fruitful topic in different scales of physics. Astrophysical environments hosting extremely strong magnetic fields, such as magnetars and neutron stars, provide natural laboratories to probe this coupling [11, 12]. Terrestrial experiments employ strong laboratory magnets, including helioscopes like CAST and the future IAXO [13, 14], which search for ALPs produced in the Sun, and haloscopes like ADMX and MADMAX [15–17], designed to detect relic ALPs constituting the galactic dark matter halo.

Precise theoretical predictions are crucial for interpreting the results of these searches and guiding future experimental design. While the tree-level Primakoff effect provides a leading-order description, quantum corrections can significantly modify the effective ALP-photon coupling, especially in the strong field regimes relevant astrophysically and experimentally [18–20]. These corrections arise from loop diagrams involving charged particles that interact with both the ALP and the external magnetic field. Calculating these effects requires a non-perturbative treatment of the charged particle propagators within the background field. This is typically achieved within the Furry picture [21], where the interaction with the external field is incorporated exactly into the propagators using techniques like Schwinger’s proper time method [22].

While the concept is established, obtaining exact analytical results for loop diagrams in arbitrary, constant magnetic fields remains a technical challenge, particularly for three-point functions like the ALP-photon-photon vertex. Previous studies often relied on approximations or specific kinematic limits. This work presents a complete calculation of the one-loop fermionic correction to the effective ALP-photon coupling in an arbitrarily strong, constant, and homogeneous magnetic field. We employ magnetically enhanced fermion propagators mentioned above and perform the loop integration without resorting to approximations concerning the field strength or the kinematics of the external particles (allowing them to be on-shell or off-shell).

The paper is structured as follows: Section 2 provides the necessary theoretical background on axions, ALPs, and their effective interactions. Section 3 details the construction of the magnetically enhanced fermion propagator using the Schwinger method. In Sec. 4, we decompose the general Lorentz structure of the ALP-photon-photon vertex in the presence of an external magnetic field. Section 5 presents the core calculation of the one-loop triangle diagram, detailing the integration techniques used to handle the Schwinger phase and the proper-time integrals. We conclude by summarizing our findings and their implications. The explicit results of the trace calculations and further details are provided in a supplementary GITHUB repository ¹.

¹<https://github.com/Ozzywtlk/Effective-ALP-Photon-Coupling-in-External-Magnetic-Fields>

2 Axions and ALPs

The theoretical motivation for axions stems from the strong CP problem in quantum chromodynamics (QCD). This problem arises from the potential inclusion of a CP-violating $\bar{\theta}$ -term in the QCD Lagrangian [23],

$$\mathcal{L}_{\text{QCD}} \supset \bar{\theta} \frac{\alpha_s}{8\pi} G_{\mu\nu}^A \tilde{G}_A^{\mu\nu}, \quad (1)$$

where α_s is the strong coupling constant, $G_{\mu\nu}^A$ is the gluon field strength tensor, $\tilde{G}_A^{\mu\nu}$ is its dual, and $\bar{\theta}$ is an angular parameter. This term contributes to the neutron's electric dipole moment (EDM), but experimental bounds [24] constrain $|\bar{\theta}| < 10^{-10}$, implying an unexpectedly small value and posing a fine-tuning problem.

To render the $\bar{\theta}$ parameter physically redundant, Peccei and Quinn proposed introducing a new, anomalous global symmetry, denoted $U(1)_{\text{PQ}}$ [25]. At high energies, this symmetry is postulated to act trivially on fields, leaving the Lagrangian invariant up to the topological term seen in Eq. (1). However, consistency requires considering the low-energy implications. According anomaly matching conditions, an anomalous global symmetry like $U(1)_{\text{PQ}}$ implies the existence of colored massless fermions in the low-energy theory [26]. As such particles are experimentally ruled out, the $U(1)_{\text{PQ}}$ symmetry must be spontaneously broken at some high energy scale, f_a , typically via the vacuum expectation value of a complex scalar field. This spontaneous symmetry breaking results in a massless Goldstone boson a , the axion, which possesses a characteristic shift symmetry. Crucially, the original $U(1)_{\text{PQ}}$ symmetry suffers from an axial anomaly due to non-perturbative QCD effects [27]. This means the associated chiral current, J_{PQ}^μ , is not conserved:

$$\partial_\mu J_{\text{PQ}}^\mu = \frac{\alpha_s}{8\pi} G_{\mu\nu}^A \tilde{G}_A^{\mu\nu}. \quad (2)$$

This anomaly directly generates an effective interaction between the axion and gluons:

$$\mathcal{L}_{\text{agg}} = \frac{a}{f_a} \frac{\alpha_s}{8\pi} G_{\mu\nu}^A \tilde{G}_A^{\mu\nu}. \quad (3)$$

When this term is added to the Lagrangian, the $\bar{\theta}$ parameter is effectively promoted to a dynamical field. Non-perturbative QCD effects generate a potential for the axion field, whose minimum dynamically cancels the original $\bar{\theta}$ term, thus solving the strong CP problem. This mechanism also generates a small mass for the axion, making it a *pseudo-Goldstone boson*, related to the scale f_a and quark masses [8]. Specifically, one obtains a mass term of the form [8]

$$m_a = -\frac{1}{f_a} \frac{\alpha_s}{4\pi} \frac{\partial}{\partial a} \langle G_{\mu\nu}^A \tilde{G}_A^{\mu\nu} \rangle \Big|_{\langle a \rangle = -f_a \bar{\theta}} \quad (4)$$

where the right hand side corresponds to the second derivative of the effective potential. The precise properties of the axion depend on the considered model, with the best-known constructions being the KSVZ [28,29] and DFSZ [30,31] models. The KSVZ model introduces vector-like quarks that are charged under $U(1)_{\text{PQ}}$, while the DFSZ model introduces an additional Higgs doublet. . A comprehensive review of the QCD axion can be found in [32].

Astrophysical observations (e.g., neutron star cooling) and cosmological considerations constrain the allowed range for f_a , typically placing it between $\sim 10^9$ GeV and $\sim 10^{18}$ GeV

[33–35]. This motivates the study of more general Axion-Like Particles (ALPs), where the mass m_a and the effective scale Λ (analogous to f_a) are treated as independent parameters. ALPs encompass the QCD axion but allow for a broader parameter space.

In an effective field theory (EFT) approach below the scale Λ , the leading interactions of ALPs involving SM fields (before electroweak symmetry breaking, EWSB) are often described by dimension-five operators [36]:

$$\mathcal{L}_{\text{eff}}^5 = \frac{\partial^\mu a}{\Lambda} \sum_f \bar{\psi}_f C_{ff} \gamma^5 \gamma_\mu \psi_f + \frac{a}{\Lambda} \left(g_s^2 C_{GG} G_{\mu\nu}^A \tilde{G}^{\mu\nu,A} + g^2 C_{WW} W_{\mu\nu}^A \tilde{W}^{\mu\nu,A} + g'^2 C_{BB} B_{\mu\nu} \tilde{B}^{\mu\nu} \right). \quad (5)$$

Here, ψ_f represents SM fermion fields, $G^{\mu\nu}$, $W^{\mu\nu}$, and $B^{\mu\nu}$ are the field strength tensors for $SU(3)_C$, $SU(2)_L$, and $U(1)_Y$ respectively, and C_{ff} , C_{GG} , C_{WW} , C_{BB} are model-dependent Wilson coefficients. The derivative coupling to fermions respects the approximate shift symmetry $a \rightarrow a + c$ expected for a pseudo-Goldstone boson. Below the EWSB scale, the W and B interactions mix, generating an effective coupling to photons:

$$\mathcal{L}_{a\gamma\gamma} = \frac{g_{a\gamma\gamma}}{4} a F_{\mu\nu} \tilde{F}^{\mu\nu}, \quad \text{with} \quad g_{a\gamma\gamma} = 4 \frac{e^2}{\Lambda} (C_{BB} + C_{WW}) \equiv 4 \frac{e^2}{\Lambda} C_{\gamma\gamma}. \quad (6)$$

This ALP-photon coupling $g_{a\gamma\gamma}$, typically treated as a free parameter and is constrained by experimental data, is the primary focus of experimental searches based on the Primakoff effect and is the central quantity investigated in this paper, including its modification by quantum effects in strong magnetic fields.

3 Enhanced Propagators in External Magnetic Fields

To account for the effects of external background fields, we adopt the Furry picture to decompose the gauge field as

$$A_\mu = A_\mu^c + A_\mu^q, \quad (7)$$

where A_μ^c denotes the classical external field, and A_μ^q is the quantized electromagnetic field. The QED Lagrangian then takes the form

$$\mathcal{L}_{\text{EM}} = -\frac{1}{4} F_{\mu\nu} \tilde{F}^{\mu\nu} + \bar{\psi} \left(\underbrace{i\cancel{\partial} - e_f \cancel{A}_c}_{=: i\cancel{\mathcal{D}}} - m \right) \psi - e \bar{\psi} \cancel{A}_q \psi, \quad (8)$$

where $F^{\mu\nu}$ is the quantized electromagnetic field strength tensor, $\tilde{F}^{\mu\nu}$ its dual, ψ the fermion field, e_f the electromagnetic charge and m the mass of a given fermion. We use slash notation to indicate the contraction of a four-vector with gamma matrices. Treating the quantum component as a perturbation, we absorb the classical part into the fermionic propagator, which we compute non-perturbatively using Schwinger's proper-time method [22].

Our goal is to explicitly calculate the Greens function satisfying the equation

$$(i\cancel{\mathcal{D}} - m) S_F(x, x') = \delta^4(x - x'). \quad (9)$$

Unfortunately, simply converting this equation into momentum space is not immediately justifiable, since the gauge field breaks the translation invariance, unless A_μ is linear in spacetime. To tackle this problem, we choose the Fock-Schwinger gauge,

$$A_\mu^c(x) = -\frac{1}{2}F_{\mu\nu}^c(x^\nu - y^\nu), \quad (10)$$

which restores the translation invariance, when $y = x'$. This chosen point fixed for every single propagator in our calculations, and therefore for higher order fermionic loops, the translation invariance of the Eq. (3) only holds on a single interaction vertex. We therefore now generalize this arbitrary gauge, and study the effects of gauge transformations on the Green's function equation. Writing local gauge transformations as

$$A_\mu(x) \rightarrow A'_\mu(x) = A_\mu(x) + \partial_\mu \alpha(x), \quad (11)$$

where $\alpha(x)$ is a scalar function, Eq. (3) becomes

$$i\delta^4(x - x') = e^{i\alpha(x)}(i\not{D} - m)e^{-i\alpha(x)}S'_F(x, x') \quad (12)$$

$$= (i\not{D} - m)e^{-i[\alpha(x) - \alpha(x')]}S'_F(x, x') \quad (13)$$

Simply put, transforming a propagator from a general gauge A_μ to a gauge A_μ^{FS} in the Fock-Schwinger gauge can be done by

$$S_F(x, x') = e^{i\Phi(x, x')} S_F^{\text{FS}}(x, x'). \quad (14)$$

with

$$\Phi(x, x') = -e_f \int_{x'}^x d\xi^\mu \left[A_\mu^c + \frac{F_{\mu\nu}^c(\xi - x')^\nu}{2} \right], \quad (15)$$

which is a gauge and spacetime dependant phase factor. The integration variable is contracted with the tensor inside of the integrand. This way, the gauge and translation dependant part is factored out of the propagator, and we can work with the translation invariant part of the propagator, by fixing the point x' suitably. To calculate S^{FS} , we take the Fourier transform of the equation (3),

$$S_F^{\text{FS}}(p) = i(\not{p} - e_f \not{A}^{\text{FS}} - m)^{-1} = (\not{p} - e_f \not{A}^{\text{FS}} + m) \int_0^\infty ds e^{is\{\not{p} - e_f \not{A}^{\text{FS}} - m^2 + i\varepsilon\}} \quad (16)$$

where we have used the mathematical identity

$$\frac{1}{C + i\varepsilon} = \int_0^\infty ds e^{is(C + i\varepsilon)}, \quad (17)$$

for $C \in \mathbb{R}$ and $\varepsilon > 0$. To bring the integral into a useful form, we multiply Eq. (16) with the Dirac operator from both sides, and get

$$\begin{aligned} 1 &= ([\not{p} - e_f \not{A}^{\text{FS}}] - m^2) \int_0^\infty ds e^{is\{\not{p} - e_f \not{A}^{\text{FS}} - m^2 + i\varepsilon\}} \\ &= \left(p^2 + e_f^2 \frac{F^{c,\mu\rho} F_\rho^{c,\nu}}{4} \frac{\partial}{\partial p^\mu} \frac{\partial}{\partial p^\nu} - m^2 + e_f \frac{F_{\mu\nu}^c \sigma^{\mu\nu}}{2} \right) \int_0^\infty ds e^{is\{\not{p} - e_f \not{A}^{\text{FS}} - m^2 + i\varepsilon\}} \end{aligned} \quad (18)$$

where $\sigma^{\mu\nu} = \frac{i}{2}[\gamma^\mu, \gamma^\nu]$. The last step is to solve this equation, which is not very insightful for our purposes. We instead refer the reader to [37] for the details. While the above formulation

$$\hat{S}_F = \text{double line with arrow} \equiv \text{single line with arrow} + \text{single line with arrow and wavy line} + \text{single line with arrow and two wavy lines} + \dots$$

Figure 1: Expansion of the enhanced fermion propagator in terms of external classical fields.

is general, explicit solutions for the propagator are known only for specific background configurations. In the case of a constant magnetic field, the fermion propagator can be expressed as [22, 38]

$$S_f(X) = e^{i\Phi(x, x')} \frac{i\beta}{2(4\pi)^2} \int_0^\infty \frac{ds}{s \sin(\beta s)} \left\{ \frac{1}{s} \left[\cos(\beta s) X_\mu \tilde{\Lambda}^{\mu\nu} \gamma_\nu + i \sin(\beta s) X_\mu \hat{F}^{\mu\nu} \gamma_\nu \gamma^5 \right] \right. \\ \left. - \frac{\beta}{\sin(\beta s)} X_\mu \tilde{\Lambda}^{\mu\nu} \gamma_\nu + m_f [2 \cos(\beta s) + \sin(\beta s) \gamma_\mu \hat{F}^{\mu\nu} \gamma_\nu] \right\} \\ \times e^{-i(m^2 s + \frac{X_\mu \tilde{\Lambda}^{\mu\nu} X_\nu}{4s} - \frac{\beta}{4 \tan(\beta s)} X_\mu \tilde{\Lambda}^{\mu\nu} X_\nu)}. \quad (19)$$

Here, $X^\mu = x^\mu - x'^\mu$, $\beta = e_f |B|$, $\Lambda^{\mu\nu} = F_{c, \mu\alpha}^\mu F_c^{\alpha\nu} / B^2$, $\tilde{\Lambda}^{\mu\nu} = \tilde{F}_{c, \mu\alpha}^\mu \tilde{F}_c^{\alpha\nu} / B^2$, $\hat{F}_c^{\mu\nu} = F_c^{\mu\nu} / |B|$, and $\hat{\tilde{F}}^{\mu\nu} = \tilde{F}^{\mu\nu} / |B|$. This propagator can be understood as the resummation of its perturbative expansion in external fields, as illustrated in Fig. 1. Due to its complexity, the perturbative expansion remains the dominant approach in practical calculations. In the following section, we utilize the enhanced propagator to construct Feynman amplitudes.

4 Lorentz Structure of the ALP-Photon-Photon Vertex

Starting from the tree-level ALP-photon interaction Lagrangian in Eq. (2), characterized by the coupling $g_{a\gamma\gamma}$, we calculate the modifications induced by an external magnetic field. These modifications arise from one-loop diagrams involving fermions interacting non-perturbatively with the background field. This leads to an effective vertex function, $\Gamma_{a\gamma\gamma}^{\mu\nu\rho}$, which manifests the field-dependent corrections, replacing the simple point-like interaction, as illustrated in Fig. 2. where the ALP momentum is denoted as k , while momenta of the two photons are p_i .

To analyze the enhanced coupling $\Gamma_{a\gamma\gamma}^{\mu\nu\rho}$, we begin by decomposing it into a basis of Lorentz structures. This decomposition simplifies the calculation, as the coefficients associated with each structure can be isolated by contracting $\Gamma_{a\gamma\gamma}^{\mu\nu\rho}$ with the corresponding basis element, provided the basis is chosen to be orthogonal. The fundamental building blocks for these structures are the external momenta k , p_1 , and p_2 . While various orthogonalization schemes exist, the presence of an external magnetic field makes it advantageous to incorporate the

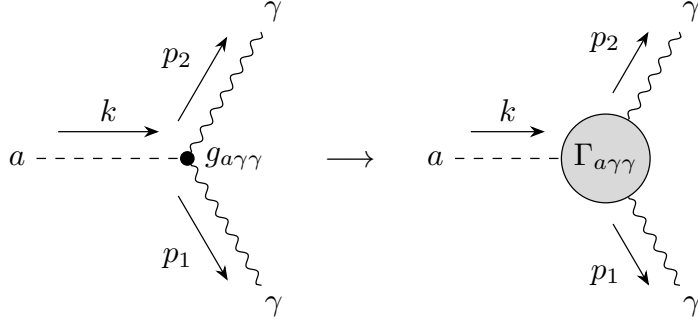


Figure 2: ALP-photon-photon coupling with (right) and without (left) external magnetic field effects.

field strength tensor $F_c^{\mu\nu}$ into the basis construction. The general Lorentz structure of the vertex can then be built from linear combinations of the following four-vectors:

$$q^\mu, \quad F_c^{\mu\nu} q_\nu, \quad F_c^{\mu\nu} F_{c,\nu\rho} q^\rho, \quad \tilde{F}_c^{\mu\nu} q_\nu, \quad (20)$$

where $q \in \{k, p_1, p_2\}$. Additional contractions with the dual field strength tensor are omitted, as they either reduce to the above structures or vanish due to the absence of external electric fields.²

To ensure mutual orthogonality and completeness, we work in the Ritus basis for the Lorentz structures [39, 40], which consists of the vectors

$$q^\mu, \quad L_q^\mu := \hat{F}_c^{\mu\nu} q_\nu, \quad \tilde{L}_q^\mu := \hat{\tilde{F}}_c^{\mu\nu} q_\nu, \quad G_q^\mu := \frac{q^2 \hat{F}_c^{\mu\nu} \hat{F}_{c,\nu\rho} q^\rho}{L_q^2} + q^\mu. \quad (21)$$

For on-shell photons ($p_i^2 = 0$), the vector $G_{p_i}^\mu$ simplifies to p_i^μ . Geometrically, these basis vectors can be drawn as projections of the external momenta parallel and perpendicular to the magnetic field, analogous to polarization vectors. For the pseudoscalar ALP, however, this basis decomposition serves primarily as a mathematical tool.

We assign the first index (μ) of the vertex tensor $\Gamma_{a\gamma\gamma}^{\mu\nu\rho}$ to the ALP's axial current and the remaining indices (ν, ρ) to the photons. allowing us to impose the Ward identities for the photons:

$$\Gamma_{a\gamma\gamma}^{\mu\nu\rho}(k, p_1, p_2) p_{1,\nu} = 0, \quad \Gamma_{a\gamma\gamma}^{\mu\nu\rho}(k, p_1, p_2) p_{2,\rho} = 0. \quad (22)$$

These identities ensure that the decomposition contains no terms proportional to p_1^ν or p_2^ρ . Additionally, Bose symmetry requires the vertex to be symmetric under the exchange of the two photons ($p_{1,\nu} \leftrightarrow p_{2,\rho}$). Incorporating these constraints, the general expansion of the

²In other Lorentz frames, acquired electric fields would be orthogonal to the magnetic field, satisfying the Lorentz-invariant cross-field condition, $\vec{E}\vec{B} = 0$.

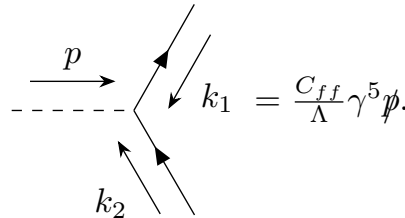
vertex in the Ritus basis is:

$$\begin{aligned}
\Gamma_{a\gamma\gamma}^{\mu\nu\rho} = & c_1 \hat{k}^\mu \hat{L}_{p_1}^\nu \hat{L}_{p_2}^\rho + c_2 \hat{k}^\mu \hat{\tilde{L}}_{p_1}^\nu \hat{\tilde{L}}_{p_2}^\rho + c_3 \hat{k}^\mu \hat{G}_{p_1}^\nu \hat{G}_{p_2}^\rho + c_4 \hat{L}_k^\mu \hat{L}_{p_1}^\nu \hat{L}_{p_2}^\rho + c_5 \hat{L}_k^\mu \hat{\tilde{L}}_{p_1}^\nu \hat{\tilde{L}}_{p_2}^\rho + c_6 \hat{L}_k^\mu \hat{G}_{p_1}^\nu \hat{G}_{p_2}^\rho \\
& + c_7 \hat{\tilde{L}}_k^\mu \hat{L}_{p_1}^\nu \hat{L}_{p_2}^\rho + c_8 \hat{\tilde{L}}_k^\mu \hat{\tilde{L}}_{p_1}^\nu \hat{\tilde{L}}_{p_2}^\rho + c_9 \hat{\tilde{L}}_k^\mu \hat{G}_{p_1}^\nu \hat{G}_{p_2}^\rho + c_{10} \hat{G}_k^\mu \hat{L}_{p_1}^\nu \hat{L}_{p_2}^\rho + c_{11} \hat{G}_k^\mu \hat{\tilde{L}}_{p_1}^\nu \hat{\tilde{L}}_{p_2}^\rho \\
& + c_{12} \hat{G}_k^\mu \hat{G}_{p_1}^\nu \hat{G}_{p_2}^\rho + \frac{c_{13}}{\sqrt{2}} \hat{k}^\mu \left(\hat{L}_{p_1}^\nu \hat{\tilde{L}}_{p_2}^\rho + \hat{\tilde{L}}_{p_1}^\nu \hat{L}_{p_2}^\rho \right) + \frac{c_{14}}{\sqrt{2}} \hat{k}^\mu \left(\hat{L}_{p_1}^\nu \hat{G}_{p_2}^\rho + \hat{G}_{p_1}^\nu \hat{L}_{p_2}^\rho \right) \\
& + \frac{c_{15}}{\sqrt{2}} \hat{k}^\mu \left(\hat{\tilde{L}}_{p_1}^\nu \hat{G}_{p_2}^\rho + \hat{G}_{p_1}^\nu \hat{\tilde{L}}_{p_2}^\rho \right) + \frac{c_{16}}{\sqrt{2}} \hat{L}_k^\mu \left(\hat{L}_{p_1}^\nu \hat{\tilde{L}}_{p_2}^\rho + \hat{\tilde{L}}_{p_1}^\nu \hat{L}_{p_2}^\rho \right) + \frac{c_{17}}{\sqrt{2}} \hat{L}_k^\mu \left(\hat{L}_{p_1}^\nu \hat{G}_{p_2}^\rho + \hat{G}_{p_1}^\nu \hat{L}_{p_2}^\rho \right) \\
& + \frac{c_{18}}{\sqrt{2}} \hat{L}_k^\mu \left(\hat{\tilde{L}}_{p_1}^\nu \hat{G}_{p_2}^\rho + \hat{G}_{p_1}^\nu \hat{\tilde{L}}_{p_2}^\rho \right) + \frac{c_{19}}{\sqrt{2}} \hat{\tilde{L}}_k^\mu \left(\hat{L}_{p_1}^\nu \hat{\tilde{L}}_{p_2}^\rho + \hat{\tilde{L}}_{p_1}^\nu \hat{L}_{p_2}^\rho \right) + \frac{c_{20}}{\sqrt{2}} \hat{\tilde{L}}_k^\mu \left(\hat{L}_{p_1}^\nu \hat{G}_{p_2}^\rho + \hat{G}_{p_1}^\nu \hat{L}_{p_2}^\rho \right) \\
& + \frac{c_{21}}{\sqrt{2}} \hat{\tilde{L}}_k^\mu \left(\hat{\tilde{L}}_{p_1}^\nu \hat{G}_{p_2}^\rho + \hat{G}_{p_1}^\nu \hat{\tilde{L}}_{p_2}^\rho \right) + \frac{c_{22}}{\sqrt{2}} \hat{G}_k^\mu \left(\hat{L}_{p_1}^\nu \hat{\tilde{L}}_{p_2}^\rho + \hat{\tilde{L}}_{p_1}^\nu \hat{L}_{p_2}^\rho \right) + \frac{c_{23}}{\sqrt{2}} \hat{G}_k^\mu \left(\hat{L}_{p_1}^\nu \hat{G}_{p_2}^\rho + \hat{G}_{p_1}^\nu \hat{L}_{p_2}^\rho \right) \\
& + \frac{c_{24}}{\sqrt{2}} \hat{G}_k^\mu \left(\hat{\tilde{L}}_{p_1}^\nu \hat{G}_{p_2}^\rho + \hat{G}_{p_1}^\nu \hat{\tilde{L}}_{p_2}^\rho \right)
\end{aligned} \tag{23}$$

Here, hats denote normalized vectors, e.g., $\hat{q}^\mu = q^\mu / \sqrt{|q^2|}$. Without specific assumptions about the CP properties governing the ALP interactions, this general decomposition cannot be reduced further. We now proceed to the explicit calculation of the one-loop diagram that determines the coefficients c_i .

5 Calculation of Magnetically Enhanced Triangle Loop

Contrary to the generally adopted strategy, we do not treat one of the field strength tensors as a classical field; instead, both are considered as quantum fields. Since there are no tree-level diagrams for ALP-photon conversion, in order to account for how the external magnetic field modifies this interaction, we must consider one-loop diagrams mediated by electromagnetically charged particles. Focusing on ALP-fermion interactions, the corresponding Feynman rule for the ALP-fermion interaction vertex in the momentum space can be derived from Eq. (2) as



$$\text{---} \xrightarrow{p} \text{---} \begin{array}{c} \nearrow k_1 \\ \searrow k_2 \end{array} = \frac{C_{ff}}{\Lambda} \gamma^5 \not{p}. \tag{24}$$

The loop diagram for the ALP-photon vertex consists of three internal fermion lines that are subject to external magnetic fields, as depicted in Fig. 3.

For the integration over the internal loop momenta, we employ the methodology presented in [41, 42], designed to obtain exact results for arbitrary magnetic field strengths. The core strategy is to evaluate the spacetime integrals first, followed by the momentum integrals, which are brought into a Gaussian form. Our calculation focuses on the vector-vector-pseudovector loop diagram, involving the shift-invariant fermion-pseudovector vertex given in Eq. (24). We define the constant magnetic field direction to be parallel to the z -axis.

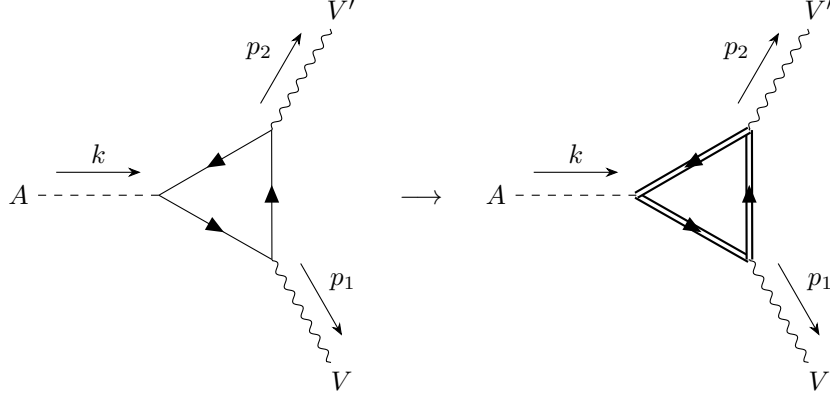


Figure 3: Triangle loop diagram for the vector-vector-axial vector coupling under the influence of external magnetic fields.

We begin by examining the properties of the phase factor $\Phi(x, x')$ from Eq. (3). The integral defining $\Phi(x, x')$ is path-independent. Consequently, for a path traversing from x' to x and then back to x' , the total phase accumulation is zero:

$$\Phi(x, x') + \Phi(x', x) = -\frac{e_f}{2} F_{\mu\nu}^c (x - x')^\nu \int_{x'}^x d\xi^\mu = -\frac{e_f}{2} F_{c,\mu\nu} (x - x')^\nu (x - x')^\mu = 0. \quad (25)$$

For a closed loop integral involving $n \geq 3$ vertices, the total Schwinger phase factor Φ_Σ generally does not vanish. As discussed in Sec. 3, each a phase factor $\Phi(x, x')$ depends on the gauge choice and the endpoints of the internal fermion line. Therefore when combining propagators in a loop, these individual phases do not necessarily cancel. In the specific case of the triangle loop ($n = 3$) relevant here, with vertices at x, y, z , the total phase factor is the sum of the phases along each leg: $\Phi_\Sigma(x, y, z) = \Phi(x, y) + \Phi(y, z) + \Phi(z, x)$. To evaluate this phase explicitly, we use the gauge freedom to choose a convenient representation for the constant magnetic field's vector potential A^c :

$$A^c = \frac{|B|}{2} (0, -y, x, 0). \quad (26)$$

In this gauge, the total phase accumulated around the loop defined by vertices at x, y, z is

$$\Phi_\Sigma(x, y, z) := -\frac{\beta}{2} \left(x_\mu \hat{F}_c^{\mu\nu} y_\nu + y_\mu \hat{F}_c^{\mu\nu} z_\nu + z_\mu \hat{F}_c^{\mu\nu} x_\nu \right). \quad (27)$$

Since this expression is generally non-zero, the manifest translation invariance (and thus momentum conservation) is obscured in this coordinate-space representation. It proves more convenient to work with the translation-invariant part of the propagator, Eq. (19), expressed in momentum space:

$$S_F(p) = \int_0^\infty \frac{ds_j}{\mathfrak{c}_j} \left[\left(m_f + \not{p}_\parallel \right) \mathfrak{e}_j + \frac{\not{p}_\perp}{\mathfrak{c}_j} \right] e^{-is \left(m_f^2 - p_\parallel^2 - p_\perp^2 \frac{\mathfrak{t}_j}{\beta s} \right)}, \quad (28)$$

where $p_{\parallel} := (p^0, 0, 0, p^3)$ and $p_{\perp} := (0, p^1, p^2, 0)$ denote the components parallel and perpendicular to the magnetic field, respectively. Note that this decomposition differs from the Ritus basis vectors L_p and \tilde{L}_p due to the index structure arising from the field strength tensor's antisymmetry. For brevity, we introduce the following abbreviations for trigonometric and exponential factors dependent on the proper-time variable s_j :

$$\begin{aligned} \mathbf{t}_j &:= \tan(\beta s_j) \\ \mathbf{c}_j &:= \cos(\beta s_j) \\ \mathbf{s}_j &:= \sin(\beta s_j) \\ \mathbf{e}_j &:= e^{i\beta s_j \Sigma_3} = \mathbf{c}_j + i\mathbf{s}_j \Sigma_3. \end{aligned} \quad (29)$$

where Σ_3 corresponds to the spin operator along the magnetic field.

With these considerations, we express the tensor-valued vertex loop integral as

$$\begin{aligned} \Gamma_{a\gamma\gamma}^{\mu\nu\rho}(k, p_1, p_2) &= -\frac{i}{2} \sum_f \frac{e_f^2 C_{ff}}{\Lambda} \iiint \frac{d^4 q}{(2\pi)^4} \frac{d^4 \ell}{(2\pi)^4} \frac{d^4 w}{(2\pi)^4} \iiint d^4 x d^4 y d^4 z \\ &\times e^{i\Phi_{\Sigma}(x,y,z)} \text{Tr} [\gamma^5 \gamma^{\mu} S_f(q) \gamma^{\nu} S_f(\ell) \gamma^{\rho} S_f(w)] \\ &\times e^{-ix(k+q-w)-iy(-p_1+w-\ell)-iz(-p_2+\ell-q)}. \end{aligned} \quad (30)$$

The spacetime integrals originate from the interaction vertices, while the momentum integrals arise from the Fourier transformation of the fermion propagators.

5.1 Integration over the Spacetime Coordinates

We note that the quantities in the phase term are all contracted with the field strength tensor, meaning that only components perpendicular to the magnetic field remain in the exponential. Therefore, we decompose the spacetime measure as

$$d^4 x = d^2 x_{\perp} d^2 x_{\parallel}, \quad (31)$$

and perform the integration over x_{\parallel} , y_{\parallel} , and z_{\parallel} . This yields

$$\begin{aligned} \Gamma_{a\gamma\gamma}^{\mu\nu\rho}(k, p_1, p_2) &= -\frac{i(2\pi)^6}{2} \sum_f \frac{e_f^2 C_{ff}}{\Lambda} \iiint \frac{d^4 q}{(2\pi)^4} \frac{d^4 \ell}{(2\pi)^4} \frac{d^4 w}{(2\pi)^4} \delta^{(2)}(k_{\parallel} + q_{\parallel} - w_{\parallel}) \\ &\times \delta^{(2)}(-p_{1\parallel} + w_{\parallel} - \ell_{\parallel}) \delta^{(2)}(-p_{2\parallel} + \ell_{\parallel} - q_{\parallel}) \text{Tr} [\gamma^5 \gamma^{\mu} S_f(q) \gamma^{\nu} S_f(\ell) \gamma^{\rho} S_f(w)] \\ &\times \underbrace{\iiint d^2 x_{\perp} d^2 y_{\perp} d^2 z_{\perp} e^{i[\Phi_{\Sigma}(x,y,z) + K_1(x,y,z)]}}_{=:A}, \end{aligned} \quad (32)$$

with

$$K_1(x, y, z) = -x_{\perp}(k_{\perp} + q_{\perp} - w_{\perp}) - y_{\perp}(-p_{1\perp} + w_{\perp} - \ell_{\perp}) - z_{\perp}(-p_{2\perp} + \ell_{\perp} - q_{\perp}) \quad (33)$$

where momentum conservation along the magnetic field is enforced by the delta functions. The remaining part of the integration requires additional evaluation, which we perform

separately for each perpendicular variable. In this specific magnetic field configuration, the action of \hat{F}_c on spacetime coordinates projects them onto the xy -plane while simultaneously rotating them by 90° around the z -axis, since $\hat{F}_c^{12} = -\hat{F}_c^{21} = 1$, with all other matrix components vanishing. This means that on the subspace perpendicular to the magnetic field, we have

$$\hat{F}_c^2 \Big|_{\perp} = -\mathbb{1}_{\perp}. \quad (34)$$

Using this property, we rewrite the phase terms in Eqs. (27) and (33) as

$$\Phi_{\Sigma}(x, y, z) = -\frac{\beta}{2} \left(x_{\perp} \hat{F}_c [y_{\perp} - z_{\perp}] + y_{\perp} \hat{F}_c z_{\perp} \right) \quad (35)$$

$$K_1(x, y, z) = x_{\perp} \hat{F}_c^2 (k_{\perp} + q_{\perp} - w_{\perp}) \underbrace{-y_{\perp}(-p_{1\perp} + w_{\perp} - \ell_{\perp}) - z_{\perp}(-p_{2\perp} + \ell_{\perp} - q_{\perp})}_{=:K_2(y,z)}. \quad (36)$$

After performing the rotation $x_{\perp} \hat{F}_c \rightarrow \tilde{x}_{\perp}$, which leaves the measure invariant, we can perform the integration over the \tilde{x}_{\perp} variable and obtain

$$\begin{aligned} A &= \left(\frac{4\pi}{\beta} \right)^2 \iint d^2 y_{\perp} d^2 z_{\perp} \delta^{(2)} \left(y_{\perp} - z_{\perp} - \frac{2\hat{F}_c}{\beta} [k_{\perp} + q_{\perp} - w_{\perp}] \right) e^{-i\frac{\beta}{2} y_{\perp} \hat{F}_c z_{\perp} + iK_2(y,z)} \\ &= \left(\frac{4\pi}{\beta} \right)^2 \int d^2 z_{\perp} e^{-i[k_{\perp} - p_{1,\perp} - p_{2,\perp}]z_{\perp} + i[k_{\perp} + q_{\perp} - w_{\perp}] \frac{2\hat{F}_c}{\beta} [-p_{1\perp} + w_{\perp} - \ell_{\perp}]} \\ &= \left(\frac{8\pi^2}{\beta} \right)^2 \delta^{(2)}(k_{\perp} - p_{1,\perp} - p_{2,\perp}) e^{i[k_{\perp} + q_{\perp} - w_{\perp}] \frac{2\hat{F}_c}{\beta} [-p_{1\perp} + w_{\perp} - \ell_{\perp}]}, \end{aligned} \quad (37)$$

where we have used $z_{\perp} \hat{F}_c z_{\perp} = 0$ in the second step. Inserting this result into Eq. (32), and performing integration over the parallel momenta, we obtain

$$\begin{aligned} \Gamma_{a\gamma\gamma}^{\mu\nu\rho}(k, p_1, p_2) &= -2 \frac{i}{(2\pi\beta)^2} \sum_f \frac{C_{ff}}{\Lambda} \iiint d^4 q d^4 \ell d^4 w \delta^{(2)}(k_{\parallel} + q_{\parallel} - w_{\parallel}) \\ &\quad \times \delta^{(2)}(-p_{1\parallel} + w_{\parallel} - \ell_{\parallel}) \delta^{(2)}(-p_{2\parallel} + \ell_{\parallel} - q_{\parallel}) \text{Tr} [\gamma^5 \gamma^{\mu} S_f(q) \gamma^{\nu} S_f(\ell) \gamma^{\rho} S_f(w)] \\ &\quad \times \delta^{(2)}(k_{\perp} - p_{1,\perp} - p_{2,\perp}) e^{i[k_{\perp} + q_{\perp} - w_{\perp}] \frac{2\hat{F}_c}{\beta} [-p_{1\perp} + w_{\perp} - \ell_{\perp}]} \\ &= -2 \frac{i}{(2\pi\beta)^2} \sum_f \frac{C_{ff}}{\Lambda} \iiint d^2 q_{\perp} d^2 \ell_{\perp} d^4 w \delta^{(4)}(k - p_2 - p_1) \\ &\quad \times \text{Tr} \left[\gamma^5 \gamma^{\mu} S_f \left(q|_{q_{\parallel}=w_{\parallel}-k_{\parallel}} \right) \gamma^{\nu} S_f \left(\ell|_{\ell_{\parallel}=w_{\parallel}-p_{1\parallel}} \right) \gamma^{\rho} S_f(w) \right] \\ &\quad \times e^{i[k_{\perp} + q_{\perp} - w_{\perp}] \frac{2\hat{F}_c}{\beta} [-p_{1\perp} + w_{\perp} - \ell_{\perp}]}. \end{aligned} \quad (38)$$

Combined with the conservation of momentum along the magnetic field, this establishes the conservation of total momentum. This result is expected, as a uniformly constant magnetic field can be interpreted as a superposition of photons in different occupation number states with an infinite wavelength, i.e., zero momentum.

5.2 Integration over the Internal Momenta

The last term in Eq. (38) is the remnant of the Schwinger phase term. For clarity, we imply the conditions $q_{\parallel} = w_{\parallel} - k_{\parallel}$ and $\ell_{\parallel} = w_{\parallel} - p_{1\parallel}$ without writing them explicitly, unless stated otherwise. We can bring the integral above into a more convenient form by expanding the propagators and rewriting the order of the integrals. We then have

$$\begin{aligned} \Gamma_{a\gamma\gamma}^{\mu\nu\rho}(k, p_1, p_2) &= -2 \frac{i}{(2\pi\beta)^2} \sum_f \frac{C_{ff}}{\Lambda} \iiint \frac{ds_1 ds_2 ds_3}{\mathbf{c}_1 \mathbf{c}_2 \mathbf{c}_3} \delta^{(4)}(k - p_2 - p_1) \\ &\times e^{-im_f^2(s_1+s_2+s_3)} \iiint d^2q_{\perp} d^2\ell_{\perp} d^4w I^{\mu\nu\rho}, \end{aligned} \quad (39)$$

with

$$\begin{aligned} I^{\mu\nu\rho} &= e^{i[k_{\perp}+q_{\perp}-w_{\perp}]\frac{2\hat{F}_c}{\beta}[-p_{1\perp}+w_{\perp}-\ell_{\perp}]} e^{is_1(w_{\parallel}-k_{\parallel})^2+is_2(w_{\parallel}-p_{1\parallel})^2+is_3w_{\parallel}^2} e^{\frac{i}{\beta}(q_{\perp}^2 t_1 + \ell_{\perp}^2 t_2 + w_{\perp}^2 t_3)} \\ &\times \text{Tr} [\gamma^5 \gamma^{\mu} \Pi_1(q) \gamma^{\nu} \Pi_2(\ell) \gamma^{\rho} \Pi_3(w)], \end{aligned} \quad (40)$$

and

$$\Pi_j(p) := (m_f + \not{p}_{\parallel}) \not{\epsilon}_j + \frac{\not{p}_{\perp}}{\mathbf{c}_j}. \quad (41)$$

We first perform the integration over the internal momenta instead of the proper time variable, and thus focus our attention on $I^{\mu\nu\rho}$. Starting with the q variable, we obtain

$$\begin{aligned} \int d^2q_{\perp} I^{\mu\nu\rho} &= C_{q_{\perp}} \int d^2q_{\perp} e^{\frac{i}{\beta}(2q_{\perp} \hat{F}_c [w_{\perp} - p_{1\perp} - \ell_{\perp}] + q_{\perp}^2 t_1)} \text{Tr} [\gamma^5 \gamma^{\mu} \Pi_1(q) \gamma^{\nu} \Pi_2(\ell) \gamma^{\rho} \Pi_3(w)] \\ &= C_{q_{\perp}} e^{-i \frac{[w_{\perp} - p_{1\perp} - \ell_{\perp}]^2}{\beta t_1}} \int d^2q_{\perp} e^{i \frac{q_{\perp}^2 t_1}{\beta}} \\ &\times \text{Tr} \left[\gamma^5 \gamma^{\mu} \Pi_1 \left(q + \frac{\hat{F}_c}{t_1} [w_{\perp} - p_{1\perp} - \ell_{\perp}] \right) \gamma^{\nu} \Pi_2(\ell) \gamma^{\rho} \Pi_3(w) \right] \\ &= -\frac{i\pi\beta}{t_1} C_{q_{\perp}} e^{-i \frac{[w_{\perp} - p_{1\perp} - \ell_{\perp}]^2}{\beta t_1}} \\ &\times \text{Tr} \left[\gamma^5 \gamma^{\mu} \Pi_1 \left(q_{\parallel} + \frac{\hat{F}_c}{t_1} [w_{\perp} - p_{1\perp} - \ell_{\perp}] \right) \gamma^{\nu} \Pi_2(\ell) \gamma^{\rho} \Pi_3(w) \right], \end{aligned} \quad (42)$$

where we have shifted $q \rightarrow q + \frac{\hat{F}_c}{t_1} [w_{\perp} - p_{1\perp} - \ell_{\perp}]$ to bring the integral into a Gaussian form. The factor $C_{q_{\perp}}$ contains terms that are not affected by the q_{\perp} integration.

An almost identical strategy is followed for ℓ_{\perp} , yielding

$$\begin{aligned} \iint d^2\ell_{\perp} d^2q_{\perp} I^{\mu\nu\rho} &= -\pi^2 \beta^2 \frac{1}{t_1 t_2 - 1} C_{\ell_{\perp}} e^{-\frac{i}{\beta} \frac{t_1}{t_1 t_2 - 1} ([w_{\perp} - k_{\perp}] \hat{F}_c + \frac{1}{t_1} [w_{\perp} - p_{1\perp}])^2} \\ &\times \left\{ \text{Tr} \left[\gamma^5 \gamma^{\mu} \Pi_1 \left(q_{\parallel} + \frac{t_2}{t_1 t_2 - 1} \hat{F}_c [w_{\perp} - p_{1\perp}] - \frac{w_{\perp} - k_{\perp}}{t_1 t_2 - 1} \right) \gamma^{\nu} \right. \right. \\ &\times \Pi_2 \left(\ell_{\parallel} - \frac{1}{t_1 t_2 - 1} [t_1 \hat{F}_c [w_{\perp} - k_{\perp}] + [w_{\perp} - p_{1\perp}]] \right) \gamma^{\rho} \Pi_3(w) \left. \right] \\ &\left. - i\beta \frac{1}{2\mathbf{c}_1 \mathbf{c}_2 (t_1 t_2 - 1)} \text{Tr} [\gamma^5 \gamma^{\mu} \gamma_{\alpha}^{\perp} \hat{F}_c^{\alpha\beta} \gamma^{\nu} \gamma_{\perp\beta} \gamma^{\rho} \Pi_3(w)] \right\}. \end{aligned} \quad (43)$$

Here, the variable shift is $\ell \rightarrow \ell - \frac{\mathbf{t}_1}{\mathbf{t}_1 \mathbf{t}_2 - 1} (\hat{F}_c[w_\perp - k_\perp] + \frac{1}{\mathbf{t}_1}[w_\perp - p_{1\perp}])$, and C_{ℓ_\perp} collects the terms unaffected by the ℓ_\perp integration. Due to the additional ℓ_\perp dependence in Eq. (42), we obtain a polynomial of order two in the ℓ_\perp variable, producing the latter trace in the result above.

Since the integral over the w variable is decoupled, we again separate the w_\perp and w_\parallel integrals. Although the w_\perp integration follows a similar structure to the previous integrals, it is quite lengthy. Therefore, we present the final result for the integration over the entire w variable:

$$\begin{aligned} \iiint d^4 w \, d^2 \ell_\perp \, d^2 q_\perp I^{\mu\nu\rho} = & \frac{i\pi^4 \beta^3}{2} \frac{e^{\frac{i}{\beta} \frac{p_{1\perp}^2 \mathbf{t}_2 \mathbf{t}_3 + p_{2\perp}^2 \mathbf{t}_1 \mathbf{t}_2 + k_\perp^2 \mathbf{t}_1 \mathbf{t}_3 + 2\mathbf{t}_1 \mathbf{t}_2 \mathbf{t}_3 k_\perp \hat{F}_c p_{1\perp}}{\mathbf{t}_1 + \mathbf{t}_2 + \mathbf{t}_3 - \mathbf{t}_1 \mathbf{t}_2 \mathbf{t}_3}}}{\mathbf{t}_1 + \mathbf{t}_2 + \mathbf{t}_3 - \mathbf{t}_1 \mathbf{t}_2 \mathbf{t}_3} \\ & \times \frac{1}{s_1 + s_2 + s_3} e^{\frac{i}{s_1 + s_2 + s_3} (s_1 s_3 k_\parallel^2 + s_2 s_3 p_{1\parallel}^2 + s_1 s_2 p_{2\parallel}^2)} \\ & \times \left(\frac{i\beta \text{Tr} [\gamma^5 \gamma^\mu \mathfrak{T}_1^{\nu\rho}]}{\mathbf{t}_1 + \mathbf{t}_2 + \mathbf{t}_3 - \mathbf{t}_1 \mathbf{t}_2 \mathbf{t}_3} - \frac{i \text{Tr} [\gamma^5 \gamma^\mu \mathfrak{T}_2^{\nu\rho}]}{s_1 + s_2 + s_3} + 2 \text{Tr} [\gamma^5 \gamma^\mu \mathfrak{T}_3^{\nu\rho}] \right) \quad (44) \end{aligned}$$

with the operators

$$\begin{aligned} \mathfrak{T}_1^{\nu\rho} &:= \frac{\eta_\perp^{\alpha\beta} + \mathbf{t}_1 \hat{F}_c^{\alpha\beta}}{\mathbf{c}_2 \mathbf{c}_3} \mathfrak{P}_1 \gamma^\nu \gamma_\alpha^\perp \gamma^\rho \gamma_\beta^\perp + \frac{\eta_\perp^{\alpha\beta} + \mathbf{t}_3 \hat{F}_c^{\alpha\beta}}{\mathbf{c}_1 \mathbf{c}_2} \gamma_\alpha^\perp \gamma^\nu \gamma_\beta^\perp \gamma^\rho \mathfrak{P}_3 + \frac{\eta_\perp^{\alpha\beta} + \mathbf{t}_2 \hat{F}_c^{\alpha\beta}}{\mathbf{c}_1 \mathbf{c}_3} \gamma_\alpha^\perp \gamma^\nu \mathfrak{P}_2 \gamma^\rho \gamma_\beta^\perp, \\ \mathfrak{T}_2^{\nu\rho} &:= \mathfrak{P}_1 \gamma^\nu \gamma_\perp^\alpha \mathbf{e}_2 \gamma^\rho \gamma_\alpha^\perp \mathbf{e}_3 + \gamma_\perp^\alpha \mathbf{e}_1 \gamma^\nu \gamma_\alpha^\perp \mathbf{e}_2 \gamma^\rho \mathfrak{P}_3 + \gamma_\perp^\alpha \mathbf{e}_1 \gamma^\nu \mathfrak{P}_2 \gamma^\rho \gamma_\alpha^\perp \mathbf{e}_3, \\ \mathfrak{T}_3^{\nu\rho} &:= \mathfrak{P}_1 \gamma^\nu \mathfrak{P}_2 \gamma^\rho \mathfrak{P}_3 \end{aligned} \quad (45)$$

where

$$\begin{aligned} \mathfrak{P}_1 &:= \Pi_1 \left(\underbrace{-\frac{s_3 k_\parallel + s_2 p_{2\parallel}}{s_1 + s_2 + s_3}}_{a_1} + \underbrace{\frac{\mathbf{t}_2 \mathbf{t}_3 \hat{F}_c p_{1\perp} - \mathbf{t}_2 p_{2\perp} - \mathbf{t}_3 k_\perp}{\mathbf{t}_1 + \mathbf{t}_2 + \mathbf{t}_3 - \mathbf{t}_1 \mathbf{t}_2 \mathbf{t}_3}}_{b_1} \right) \\ \mathfrak{P}_2 &:= \Pi_2 \left(\underbrace{\frac{s_1 p_{2\parallel} - s_3 p_{1\parallel}}{s_1 + s_2 + s_3}}_{a_2} + \underbrace{\frac{-\mathbf{t}_1 \mathbf{t}_3 \hat{F}_c k_\perp - \mathbf{t}_3 p_{1\perp} + \mathbf{t}_1 p_{2\perp}}{\mathbf{t}_1 + \mathbf{t}_2 + \mathbf{t}_3 - \mathbf{t}_1 \mathbf{t}_2 \mathbf{t}_3}}_{b_2} \right) \\ \mathfrak{P}_3 &:= \Pi_3 \left(\underbrace{\frac{s_2 p_{1\parallel} + s_1 k_\parallel}{s_1 + s_2 + s_3}}_{a_3} + \underbrace{\frac{\mathbf{t}_1 \mathbf{t}_2 \hat{F}_c p_{2\perp} + \mathbf{t}_1 k_\perp + \mathbf{t}_2 p_{1\perp}}{\mathbf{t}_1 + \mathbf{t}_2 + \mathbf{t}_3 - \mathbf{t}_1 \mathbf{t}_2 \mathbf{t}_3}}_{b_3} \right). \end{aligned}$$

Evaluation of these traces is performed using the MATHEMATICA package FEYN CALC [43]. Due to the presence of γ^5 matrices, the results consist of contractions of external momenta with Levi-Civita tensors. These can be further reduced by using the symmetry condition that $\Gamma_{a\gamma\gamma}^{\mu\nu\rho}$ must be symmetric under the exchange of the ν and ρ indices. As an example, we give the result of the shortest trace explicitly:

$$\text{Tr} [\gamma^5 \gamma^\mu \mathfrak{T}_1^{\nu\rho}] = 4i \left[\mathbf{t}_1 \frac{\left(\eta_\perp^{\alpha\nu} \hat{F}_c^{\mu\rho} - \eta_\perp^{\nu\mu} \hat{F}_c^{\alpha\rho} \right) (b_{1,\alpha} - \mathbf{c}_1 a_{1,\alpha}) + a_{1,\alpha} \mathbf{s}_1 \hat{F}_c^{\mu\nu} \hat{F}_c^{\alpha\rho}}{\mathbf{c}_2 \mathbf{c}_3} \right]$$

$$\begin{aligned}
& + \mathbf{t}_2 \frac{\left(\eta_{\perp}^{\alpha\nu} \hat{F}_c^{\mu\rho} + \eta_{\perp}^{\alpha\rho} \hat{F}_c^{\mu\nu} + \eta_{\perp}^{\nu\rho} \hat{F}_c^{\alpha\mu} \right) (b_{2,\alpha} - \mathbf{c}_2 a_{2,\alpha})}{\mathbf{c}_1 \mathbf{c}_3} \\
& - \mathbf{t}_3 \frac{\left(\eta_{\perp}^{\alpha\rho} \hat{F}_c^{\mu\nu} - \eta_{\perp}^{\mu\rho} \hat{F}_c^{\alpha\nu} \right) (b_{3,\alpha} + \mathbf{c}_3 a_{3,\alpha}) + a_{3,\alpha} \mathbf{s}_3 \hat{F}_c^{\mu\rho} \hat{F}_c^{\alpha\nu}}{\mathbf{c}_1 \mathbf{c}_2} \Big] \\
& \equiv \frac{1}{\mathbf{c}_1 \mathbf{c}_2 \mathbf{c}_3} \sum_{i=1}^3 \mathbf{s}_i \left(a_{i,\alpha} \left[\mathbf{c}_i C_{1,i}^{\alpha\mu\nu\rho} + \mathbf{s}_i C_{2,i}^{\alpha\mu\nu\rho} \right] + b_{i,\alpha} C_{3,i}^{\alpha\mu\nu\rho} \right). \tag{46}
\end{aligned}$$

The above expression is a shorthand decomposition that we introduce to facilitate the integration. The individual tensors in Eq. (46) correspond to lengthy linear combinations of products of Levi-Civita tensors and metric tensors, which do not depend on any remaining integration variables. Similar shorthand decompositions can be obtained for the remaining traces in Eq. (44), yielding

$$\begin{aligned}
\text{Tr} \left[\gamma^5 \gamma^{\mu} \mathfrak{T}_2^{\nu\rho} \right] &= \mathbf{c}_1 \mathbf{c}_2 \mathbf{c}_3 \sum_{i=1}^3 \left(a_{i,\alpha} \left[\mathbf{t}_1 C_{4,i}^{\alpha\mu\nu\rho} + \mathbf{t}_2 C_{5,i}^{\alpha\mu\nu\rho} + \mathbf{t}_3 C_{6,i}^{\alpha\mu\nu\rho} + \mathbf{t}_1 \mathbf{t}_2 C_{7,i}^{\alpha\mu\nu\rho} + \mathbf{t}_1 \mathbf{t}_3 C_{8,i}^{\alpha\mu\nu\rho} \right. \right. \\
& \quad \left. \left. + \mathbf{t}_2 \mathbf{t}_3 C_{9,i}^{\alpha\mu\nu\rho} + \mathbf{t}_1 \mathbf{t}_2 \mathbf{t}_3 C_{10,i}^{\alpha\mu\nu\rho} \right] + \frac{b_{i,\alpha}}{\mathbf{c}_i} \left[\mathbf{t}_1 C_{11,i}^{\alpha\mu\nu\rho} + \mathbf{t}_2 C_{12,i}^{\alpha\mu\nu\rho} + \mathbf{t}_3 C_{13,i}^{\alpha\mu\nu\rho} \right. \right. \\
& \quad \left. \left. + \mathbf{t}_1 \mathbf{t}_2 C_{14,i}^{\alpha\mu\nu\rho} + \mathbf{t}_1 \mathbf{t}_3 C_{15,i}^{\alpha\mu\nu\rho} + \mathbf{t}_2 \mathbf{t}_3 C_{16,i}^{\alpha\mu\nu\rho} \right] \right), \tag{47}
\end{aligned}$$

and

$$\begin{aligned}
\text{Tr} \left[\gamma^5 \gamma^{\mu} \mathfrak{T}_3^{\nu\rho} \right] &= \mathbf{c}_1 \mathbf{c}_2 \mathbf{c}_3 \left(a_{1,\alpha} a_{2,\beta} a_{3,\tau} \left[D_1^{\alpha\beta\tau\mu\nu\rho} + \mathbf{t}_1 D_2^{\alpha\beta\tau\mu\nu\rho} + \mathbf{t}_2 D_3^{\alpha\beta\tau\mu\nu\rho} + \mathbf{t}_3 D_4^{\alpha\beta\tau\mu\nu\rho} \right. \right. \\
& \quad \left. \left. + \mathbf{t}_1 \mathbf{t}_2 D_5^{\alpha\beta\tau\mu\nu\rho} + \mathbf{t}_1 \mathbf{t}_3 D_6^{\alpha\beta\tau\mu\nu\rho} + \mathbf{t}_2 \mathbf{t}_3 D_7^{\alpha\beta\tau\mu\nu\rho} + \mathbf{t}_1 \mathbf{t}_2 \mathbf{t}_3 D_8^{\alpha\beta\tau\mu\nu\rho} \right] \right. \\
& \quad + \frac{b_{1,\alpha} a_{2,\beta} a_{3,\tau}}{\mathbf{c}_1} \left[D_9^{\alpha\beta\tau\mu\nu\rho} + \mathbf{t}_2 D_{10}^{\alpha\beta\tau\mu\nu\rho} + \mathbf{t}_3 D_{11}^{\alpha\beta\tau\mu\nu\rho} + \mathbf{t}_2 \mathbf{t}_3 D_{12}^{\alpha\beta\tau\mu\nu\rho} \right] \\
& \quad + \frac{a_{1,\alpha} b_{2,\beta} a_{3,\tau}}{\mathbf{c}_2} \left[D_{13}^{\alpha\beta\tau\mu\nu\rho} + \mathbf{t}_1 D_{14}^{\alpha\beta\tau\mu\nu\rho} + \mathbf{t}_3 D_{15}^{\alpha\beta\tau\mu\nu\rho} + \mathbf{t}_1 \mathbf{t}_3 D_{16}^{\alpha\beta\tau\mu\nu\rho} \right] \\
& \quad + \frac{a_{1,\alpha} a_{2,\beta} b_{3,\tau}}{\mathbf{c}_3} \left[D_{17}^{\alpha\beta\tau\mu\nu\rho} + \mathbf{t}_1 D_{18}^{\alpha\beta\tau\mu\nu\rho} + \mathbf{t}_2 D_{19}^{\alpha\beta\tau\mu\nu\rho} + \mathbf{t}_1 \mathbf{t}_2 D_{20}^{\alpha\beta\tau\mu\nu\rho} \right] \\
& \quad + \frac{b_{1,\alpha} b_{2,\beta} a_{3,\tau}}{\mathbf{c}_1 \mathbf{c}_2} \left[D_{21}^{\alpha\beta\tau\mu\nu\rho} + \mathbf{t}_3 D_{22}^{\alpha\beta\tau\mu\nu\rho} \right] + \frac{b_{1,\alpha} a_{2,\beta} b_{3,\tau}}{\mathbf{c}_1 \mathbf{c}_3} \left[D_{23}^{\alpha\beta\tau\mu\nu\rho} + \mathbf{t}_2 D_{24}^{\alpha\beta\tau\mu\nu\rho} \right] \\
& \quad + \frac{a_{1,\alpha} b_{2,\beta} b_{3,\tau}}{\mathbf{c}_2 \mathbf{c}_3} \left[D_{25}^{\alpha\beta\tau\mu\nu\rho} + \mathbf{t}_1 D_{26}^{\alpha\beta\tau\mu\nu\rho} \right] + \frac{b_{1,\alpha} b_{2,\beta} b_{3,\tau}}{\mathbf{c}_1 \mathbf{c}_2 \mathbf{c}_3} D_{27}^{\alpha\beta\tau\mu\nu\rho} \\
& \quad + m_f^2 \sum_{i=1}^3 \left(a_{i,\alpha} \left[\mathbf{t}_1 C_{17,i}^{\alpha\mu\nu\rho} + \mathbf{t}_2 C_{18,i}^{\alpha\mu\nu\rho} + \mathbf{t}_3 C_{19,i}^{\alpha\mu\nu\rho} + \mathbf{t}_1 \mathbf{t}_2 C_{20,i}^{\alpha\mu\nu\rho} + \mathbf{t}_1 \mathbf{t}_3 C_{21,i}^{\alpha\mu\nu\rho} \right. \right. \\
& \quad \left. \left. + \mathbf{t}_2 \mathbf{t}_3 C_{22,i}^{\alpha\mu\nu\rho} + \mathbf{t}_1 \mathbf{t}_2 \mathbf{t}_3 C_{23,i}^{\alpha\mu\nu\rho} \right] + \frac{b_{i,\alpha}}{\mathbf{c}_i} \left[\mathbf{t}_1 C_{24,i}^{\alpha\mu\nu\rho} + \mathbf{t}_2 C_{25,i}^{\alpha\mu\nu\rho} + \mathbf{t}_3 C_{26,i}^{\alpha\mu\nu\rho} \right. \right. \\
& \quad \left. \left. + \mathbf{t}_1 \mathbf{t}_2 C_{27,i}^{\alpha\mu\nu\rho} + \mathbf{t}_1 \mathbf{t}_3 C_{28,i}^{\alpha\mu\nu\rho} + \mathbf{t}_2 \mathbf{t}_3 C_{29,i}^{\alpha\mu\nu\rho} \right] \right). \tag{48}
\end{aligned}$$

Explicit expressions for the tensors $C_{i,j}^{\alpha\mu\nu\rho}$ and $D_i^{\alpha\beta\tau\mu\nu\rho}$ can be found in the MATHEMATICA notebook file located in the aforementioned GITHUB page. Combined with Eq. (44), we see that parts of the integrand that depend on the proper time variable consist of powers of trigonometric functions and a complicated exponential function.

5.3 Proper Time Integrals

Our goal is to provide an exact solution that can be numerically computed for all combinations of perpendicular momenta and magnetic field strengths, while allowing suitable approximations in different regimes. We begin by changing the integration variables as

$$\beta s_1 \rightarrow s v_1, \quad \beta s_2 \rightarrow s v_2, \quad \text{and} \quad \beta s_3 \rightarrow s(1 - v_1 - v_2) \equiv s v_3,$$

with the integration domain given by

$$(s, v_1, v_2) \in \mathbb{R}_{\geq 0} \times \{(v_1, v_2) \mid 0 \leq v_1 \leq 1, 0 \leq v_2 \leq 1 - v_1\}. \quad (49)$$

We first integrate over the s variable by treating it as a complex number, and then perform the remaining v_i integrals numerically. By expanding the trace result obtained above, we obtain proper time integrals of the form

$$K \int ds \underbrace{\csc^n(s) T_0 s^m e^{\frac{i}{\beta} \csc(s) [p_{1\perp}^2 T_1 + p_{2\perp}^2 T_2 + k_{\perp}^2 T_3 + 2k_{\perp} \hat{F}_c p_{1\perp} T_4]} e^{isP(v_1, v_2)}}_{=: J_{n,m,T_0}(s, v_1, v_2)},$$

with

$$P(v_1, v_2) = \frac{1}{\beta} [v_1 v_3 k_{\parallel}^2 + v_2 v_3 p_{1\parallel}^2 + v_1 v_2 p_{2\parallel}^2 - m_f^2], \quad (50)$$

where K is independent of s , the T_i are products of sine and cosine functions of s , v_1 , and v_2 , and $n, m \in \mathbb{Z}$. Essential singularities from the complicated exponential in Eq. (44), as well as poles from the trace term, are all located on the real axis at values $s \in \mathbb{Z}^* \pi$. Since we are only interested in the positive real axis, we use an integration path resembling a quarter circle, as illustrated in Fig. 4.

To be rigorous, we fix the external momenta and use a path-valued function of the v_1 and v_2 variables, since the behavior of the quarter circle for $R \rightarrow \infty$ and $\varepsilon \rightarrow 0$ can vary over different subdomains and external momenta. We decompose a general path as

$$C_R = C_{\text{Arc}} \cup C_{\text{Im}} \cup C_{\text{Re}, \varepsilon} \bigcup_{r=1}^{\lfloor \frac{R}{\pi} \rfloor} C_{\varepsilon, r},$$

where C_{Arc} is the quarter-circle with radius R , C_{Im} is the path along the imaginary axis, $C_{\text{Re}, \varepsilon}$ is the path along the real axis with periodic gaps of diameter 2ε around the poles, and for each $r \in \{1, \dots, \lfloor \frac{R}{\pi} \rfloor\}$, $C_{\varepsilon, r}$ is a semicircle of radius ε circumventing the r -th pole. (We do not assume any particular orientation for these paths at this stage.)

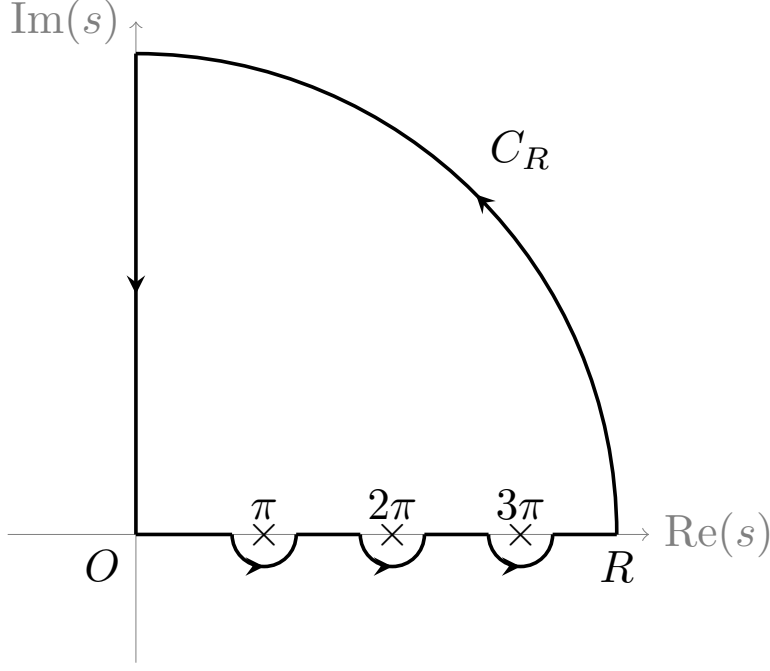


Figure 4: A possible contour of integration for the proper-time integral given in Eq. (39), for a given subdomain of the v_1 and v_2 variables.

We first determine the orientation of C_{Arc} by setting $s \rightarrow Re^{i\theta}$ with $\theta \in [0, \frac{\pi}{2}]$ (first quadrant) or $\theta \in [-\frac{\pi}{2}, 0]$ (fourth quadrant). In this case, the magnitude of each possible trigonometric product is bounded by

$$\begin{aligned}
|\csc^n[Re^{i\theta}]T_i| &\leq \frac{\cosh[kv_1 R \sin(\theta)] \cosh[kv_2 R \sin(\theta)] \cosh[kv_3 R \sin(\theta)]}{|\sinh^n(R \sin(\theta))|} \\
&\leq \frac{e^{kR \sin(\theta)}}{|\sinh^n(R \sin(\theta))|} \\
&\leq 2^n \frac{e^{nR \sin(\theta)}}{|e^{R \sin(\theta)} - e^{-R \sin(\theta)}|^n} \xrightarrow{R \rightarrow \infty} 2^n,
\end{aligned} \tag{51}$$

where $0 < k \leq n \leq 4$. This bound is independent of θ and n . Consequently, the exponential function with trigonometric arguments is also bounded in this limit. On the other hand, we obtain a polynomial in s of order m , resulting in an overall divergence of order R^{m+1} (the additional linear divergence arises from the change of variables, $ds = iRe^{i\theta}d\theta$). The remaining non-trigonometric exponential must vanish faster than $R^{-(m+1)}$. In fact,

$$\left| e^{iRe^{i\theta}P(v_1, v_2)} \right| = e^{-R \sin(\theta)P(v_1, v_2)}, \tag{52}$$

which vanishes exponentially as $R \rightarrow \infty$, provided that the overall sign of the exponent is negative. This condition depends on the external momenta, the fermion mass, and the values of v_i , which in turn determine the path orientation.

A similar discussion applies to the behavior along $C_{\varepsilon, r}$. Setting $s \rightarrow r\pi + \varepsilon e^{i\theta}$ with $\theta \in [0, \pi]$ (upper semicircle) or $\theta \in [-\pi, 0]$ (lower semicircle), the magnitude of the term

with the linear exponent converges to one as $\varepsilon \rightarrow 0$. However, the trigonometric functions, specifically \csc^n , diverge in this limit because the semicircles are centered around the poles. Expanding $\csc^n(s)$ around $s = r\pi$ for very small ε , we find

$$|\csc^n[r\pi + \varepsilon e^{i\theta}]T_i| \approx \frac{|T_i|_{s=r\pi}}{\varepsilon^n}. \quad (53)$$

Combined with the extra factor of ε from the change of variables, we require the remaining exponential function to vanish faster than ε^{n-1} . Explicitly,

$$\left| e^{\frac{i}{\beta} \csc[Re^{i\theta}][p_{1\perp}^2 T_1 + p_{2\perp}^2 T_2 + k_{\perp}^2 T_3 + 2k_{\perp} \hat{F}_c p_{1\perp} T_4]} \right| \approx e^{\frac{(-1)^r}{\beta} \frac{\sin(\theta)}{\varepsilon} [p_{1\perp}^2 T_1 + p_{2\perp}^2 T_2 + k_{\perp}^2 T_3 + 2k_{\perp} \hat{F}_c p_{1\perp} T_4]_{s=r\pi}}, \quad (54)$$

which vanishes exponentially as $\varepsilon \rightarrow 0$, depending on the sign of the exponent. This result is crucial, as it indicates that some of the poles must be dynamically excluded.

To construct a compact general result, we define the exclusion functions

$$f_{\text{Arc}} := \text{sgn}(P(v_1, v_2)), \quad (55)$$

$$f_r := \frac{1 + f_{\text{Arc}} \cdot \text{sgn}\left(\frac{(-1)^r}{e_f} \left[p_{1\perp}^2 T_1 + p_{2\perp}^2 T_2 + k_{\perp}^2 T_3 + 2k_{\perp} \hat{F}_c p_{1\perp} T_4\right]_{s=r\pi}\right)}{2}. \quad (56)$$

Using these functions, the general result of the proper-time integral for a specific J_{n,T_0} can be written as

$$\int_0^\infty ds J_{n,m,T_0}(s, v_1, v_2) = i \int_0^{f_{\text{Arc}} \cdot \infty} ds J_{n,m,T_0}(is, v_1, v_2) + 2\pi i \sum_{r=1}^\infty f_r \text{Res}_{s=r\pi} [J_{n,m,T_0}]. \quad (57)$$

Since there are no poles along the imaginary axis, the first integral on the right-hand side of Eq. (57) can be evaluated numerically without difficulty. As an example for the second term, we compute the residues for the integral corresponding to the tensor $C_{1,1}^{\alpha\mu\nu\rho}$, i.e., the case where

$$\csc^n(s)T_0 = \frac{\mathfrak{s}_1 \mathfrak{c}_1}{[(\mathfrak{c}_1 \mathfrak{c}_2 \mathfrak{c}_3)(\mathfrak{t}_1 + \mathfrak{t}_2 + \mathfrak{t}_3 - \mathfrak{t}_1 \mathfrak{t}_2 \mathfrak{t}_3)]^2} = \csc^2(s) \frac{\sin(2sv_1)}{2}, \quad (58)$$

with $n = 2$ and $m = 1$. Due to the \csc functions present, the Laurent series around the poles has a convergence radius of π , meaning that we must expand the series around each pole individually. Using the multinomial theorem combined with the generalized Cauchy product, we find the coefficients for the exponential term. The result can be summarized as

$$\begin{aligned} \text{Res}_{s=r\pi} [J_{1,1,T_0}] &= \sum_{l=0}^\infty \sum_{k=0}^{l+1} \sum_{j=0}^k \frac{i^l (-1)^{\frac{j}{2}+1+\lfloor \frac{k-j}{2} \rfloor} 2^j (j-1) B_j}{l! j! (k-j)!} a_{k-j}(2v_1) \\ &\times \left(r\pi c_{l-k+1} + \sum_{m=0}^{l-k} c_m \frac{(iP(v_1, v_2)r\pi)^{l-k-m} e^{ir\pi P(v_1, v_2)} [1 + l - k - m + iP(v_1, v_2)]}{(2 - k + l - m)!} \right), \end{aligned} \quad (59)$$

with

$$a_n(\omega) := \sin(r\pi\omega)^{\frac{1+(-1)^n}{2}} \cos(r\pi\omega)^{\frac{1-(-1)^n}{2}} \omega^n, \quad (60)$$

$$b_n(\omega) := [-\sin(r\pi\omega)]^{\frac{1+(-1)^n}{2}} \cos(r\pi\omega)^{\frac{1+(-1)^n}{2}} \omega^n, \quad (61)$$

$$c_0 := d_0^l, \quad (62)$$

$$c_m := \frac{1}{md_0} \sum_{n=1}^m (nl - m + n) c_n d_{m-n}, \quad (63)$$

$$\begin{aligned} d_m := \sum_{n=0}^m \frac{B_n i^n (-1)^{r+\lfloor \frac{m-n}{2} \rfloor} (1-2^{n-1})}{n!(m-n)!2} & \left[2p_{1\perp}^2 b_{m-n}(2v_1 + 2v_2 - 1) - 2k_{\perp}^2 b_{m-n}(1) \right. \\ & + k_{\perp} \hat{F}_c p_{1\perp} [a_{m-n}(2v_1 + 2v_2 - 1) + a_{m-n}(1 - 2v_2) - a_{m-n}(2v_1 - 1) - a_{m-n}(1)] \\ & \left. + 2p_{2\perp}^2 b_{m-n}(2v_1 - 1) \right]. \end{aligned} \quad (64)$$

Here, B_j is the j -th Bernoulli number. Although this expression may seem tedious—especially given that there are 57 other tensors to evaluate—it is not problematic because the sequences a_n , b_n , c_n , and d_n are identical across all tensors, with the only differences arising from the first term in Eq. (59). Furthermore, since these coefficients are reused repeatedly, one can employ *memoization* techniques to speed up the computation. Although the summation above does not have a closed form, one can use as many terms in the expression as needed to achieve the desired precision. The speed of convergence increases proportionally to the strength of the magnetic field. Furthermore, considering the conservation of momentum at the vertex, the exclusion function f_r turns out to be independent on the order of the pole, r , meaning either all poles are included in the integration for a given (v_1, v_2) pair, or none of them are. This allows us to sum over all poles at once, and numerically integrate the acquired closed form afterwards. For example, assuming $l = 0$, the residue from the Eq. (59) can be summed as

$$\begin{aligned} \sum_{r=1}^{\infty} \text{Res}_{s=r\pi} [J_{1,1,T_0}] &= -\frac{-2\pi \sin(2\pi v_1) P(v_1, v_2) \sin(\pi P(v_1, v_2)) + 4\pi v_1 + \sin(4\pi v_1)}{8[\cos(\pi P(v_1, v_2)) - \cos(2\pi v_1)]^2} \\ &\quad - \frac{2(\sin(2\pi v_1) + 2\pi v_1 \cos(2\pi v_1)) \cos(\pi P(v_1, v_2))}{8[\cos(\pi P(v_1, v_2)) - \cos(2\pi v_1)]^2} \end{aligned} \quad (65)$$

Closed form expressions for the remaining tensors ($l = 0$) can also be found in the MATHEMATICA notebook in the GITHUB page.

6 Discussion

We now briefly discuss the implications of the results derived in the preceding sections. The calculated magnetically enhanced vertex tensor, $\Gamma_{a\gamma\gamma}^{\mu\nu\rho}$, represents the core quantity encapsulating the quantum corrections to the ALP-photon interaction within the external magnetic field. This tensor serves as the fundamental input for computing physical observables, such

as the decay rate of ALPs into photons or the probability of photon-ALP conversion, within an effective Lagrangian framework. The magnitude and structure of these observables are inherently sensitive to the underlying model parameters, specifically the fermion-specific Wilson coefficients C_{ff} , the intrinsic vacuum ALP-photon coupling $g_{a\gamma\gamma}$, and the effective scale Λ , as indicated by Eq. 2.

To gain concrete insight into the behavior of the vertex tensor $\Gamma_{a\gamma\gamma}^{\mu\nu\rho}$, we examine its properties under specific kinematic conditions and field strengths. While the general Lorentz decomposition in Eq. (4) is extensive, it simplifies considerably in certain limits. For instance, taking photons on-shell ($p_1^2 = p_2^2 = 0$) causes exactly half of the coefficients c_i to vanish, reducing the complexity of the tensor structure. To illustrate the impact of strong magnetic

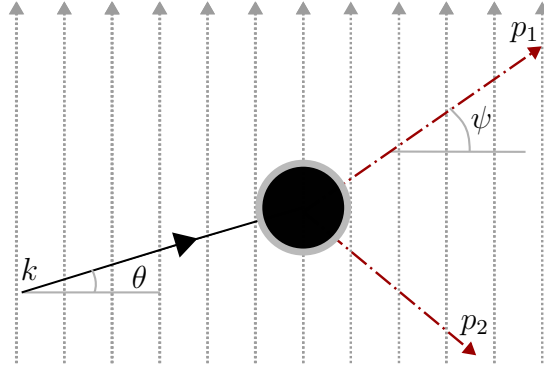


Figure 5: Sketch of ALP decay kinematics ($a \rightarrow \gamma\gamma$) in a uniform external magnetic field (grey arrows). The angle θ represents the angle between the incoming ALP's momentum and the magnetic field. Similarly, the angle ψ represents the angle between the momentum of one of the outgoing photons and the magnetic field. The direction of the second photon is determined by the principle of momentum conservation.

fields, such as those encountered in astrophysical environments like magnetars, we evaluate the remaining coefficients under specific, representative conditions. We choose a magnetic field strength where the scale is comparable to the down quark mass squared, $\beta \sim m_d^2$, similar to field strengths inferred for objects like magnetar SGR 1806-20 [44]. Furthermore, we set the ALP center-of-mass energy to the electron mass ($E_a = m_e$) as a reference scale and adopt a GUT UV-completion scale $\Lambda = 10^{19}$ eV, motivated by string theory considerations [9, 45]. It is important to emphasize that these are illustrative parameter choices designed to explore the qualitative behavior of the vertex function.

Figure 6 presents the sum of the squared Lorentz structure coefficients, effectively proportional to the squared amplitude $|\Gamma_{a\gamma\gamma}|^2$, as a function of the incoming ALP's angle θ relative to the magnetic field direction. Different curves correspond to various fixed values of ψ , the angle between one of the outgoing photon's momentum and the magnetic field. Angles θ and ψ are sketched in Fig. 6. The calculation does not average over the final photon states.

A striking feature is the maximization of the squared amplitude when the incoming ALP momentum is parallel to the magnetic field direction ($|\theta| = \frac{\pi}{2}$). This suggests a significantly enhanced interaction rate for ALPs traversing parallel to strong magnetic fields. Conversely,

for other angles, the magnitude decreases substantially, highlighting a strong directional dependence induced by the field. The plot also reveals non-trivial features, including slight oscillations for certain ψ values. While the peak magnitude at $|\theta| = \frac{\pi}{2}$ appears to be relatively insensitive to the outgoing photon angle ψ , the overall angular profile exhibits a non-linear dependence on ψ , differing notably between positive and negative ψ values. This indicates that while the distributions are symmetric around $\theta = 0$, the graphs of outgoing photons asymmetrically modulated by the field. To further explore the angular distribution of the

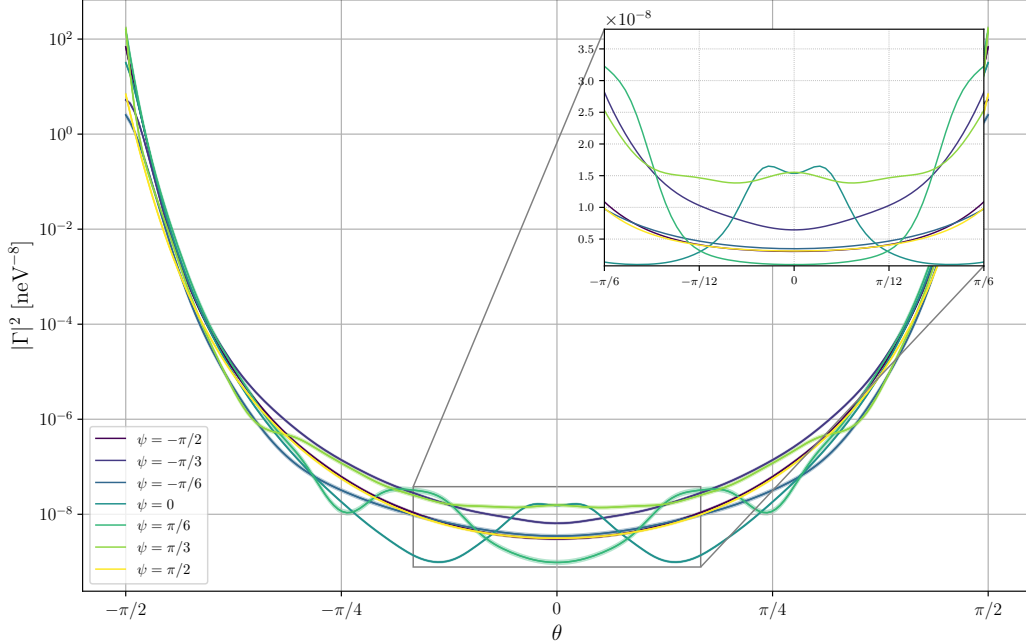


Figure 6: Sum of the squared Lorentz structure coefficients as a function of θ , shown on a logarithmic scale. The inset displays the region $|\theta| \leq \pi/6$ on a linear scale. Shaded regions indicate numerical integration errors.

interaction products, Fig. 7 displays the sum of squared coefficients as a function of the outgoing photon angle ψ for several fixed values of the incoming ALP angle θ . This provides a complementary perspective on the process kinematics, focusing on the emission pattern for a given initial ALP trajectory. We observe that the angular distribution of the outgoing photons is highly dependent on the incoming ALP angle θ . Notably, for most values of θ , the distributions are not symmetric around $\psi = 0$. Instead, they exhibit an irregular skewness. An exception occurs for $\theta = -\frac{\pi}{2}$, where the distribution appears symmetric around $\psi = 0$, while for $\theta = \frac{\pi}{2}$ the graph is maximally asymmetric. This skewness implies that photon emission is preferentially directed depending on the initial ALP angle relative to the field lines, a factor potentially relevant for detection strategies. Obtaining the full numerical value of the vertex tensor requires contracting the detailed trace results presented in Eq. (5.2) with the 57 relevant tensor structures identified in the Lorentz decomposition, followed by the final integrations over the proper-time parameters v_1 and v_2 . The complicated nature

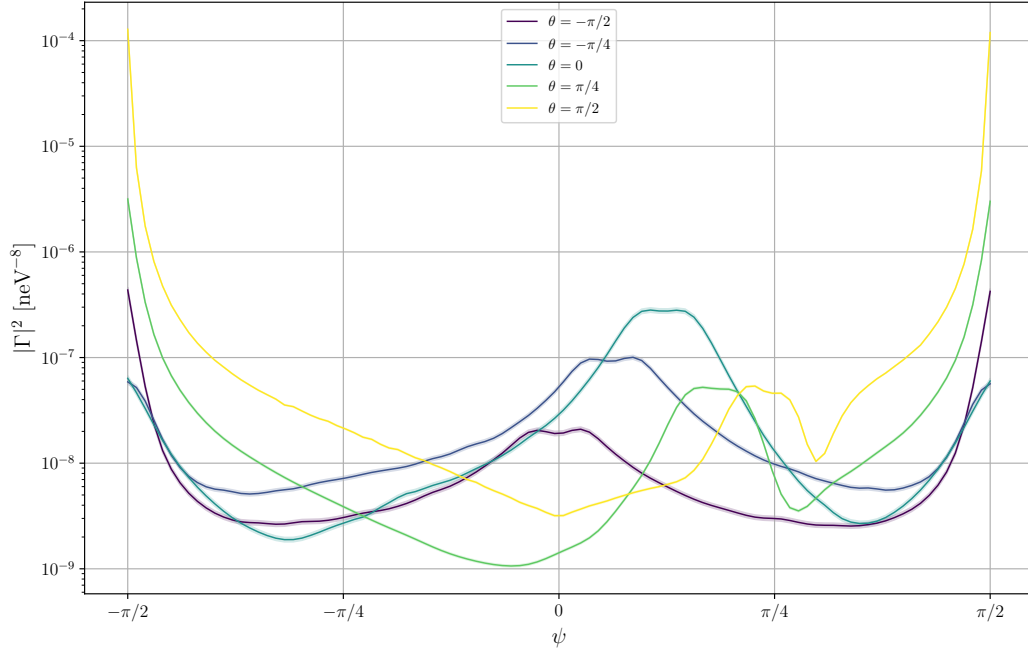


Figure 7: Sum of the squared Lorentz structure coefficients as a function of ψ , shown on a logarithmic scale. Shaded regions indicate numerical integration errors.

of the resulting integrand necessitates numerical methods for these final two-dimensional integrals. We employed the adaptive Monte Carlo integration algorithm VEGAS [46] for this task. The practical implementation involved translating the symbolic expressions, initially derived and manipulated using MATHEMATICA, into efficient C code suitable for numerical computation. It is crucial to reiterate that the numerical examples presented here rely on a first-order approximation ($l = 0$) of the residue series expansion given in Eq. (5.3). While this provides a valuable illustration of the qualitative behavior, the developed framework allows, in principle, for the inclusion of higher-order terms to achieve greater numerical precision where required. The convergence properties, as noted, are expected to improve with increasing magnetic field strength.

7 Summary

In summary, this paper presents a detailed calculation of the one-loop fermionic correction to the effective ALP-photon coupling in the presence of an arbitrary, constant, homogeneous magnetic field. Motivated by the importance of this coupling for ALP detection via the Primakoff effect in astrophysical and terrestrial settings, we aimed to provide an exact result beyond approximations previously considered in the literature.

We employed the Furry picture and utilized fermion propagators dressed by the external magnetic field, derived using Schwinger's proper-time method. The Lorentz structure of the

resulting effective vertex tensor, $\Gamma_{a\gamma\gamma}^{\mu\nu\rho}$, was systematically decomposed using the Ritus basis, which naturally incorporates the external field. The core of the work involved the explicit evaluation of the triangle loop diagram. We performed the spacetime and momentum integrations exactly following the methods presented in [41, 42], carefully handling the Schwinger phase factor arising from the non-perturbative propagators.

The final expression for the vertex tensor involves integrals over three proper-time variables. The integral over the total proper time was addressed using contour integration techniques, yielding a result composed of an integral along the imaginary axis and a sum over residues from poles located on the real axis. While the explicit expressions for these residues are fairly complicated, we outlined how they can be summed and evaluated numerically. An illustrative case, considering $\beta \sim m_d^2$, demonstrated the dependence of the squared vertex tensor magnitude on the angles of the incoming ALP and outgoing photons relative to the magnetic field.

The numerical evaluation reveals significant modifications to the ALP-photon coupling in strong magnetic fields, characterized by strong angular dependencies and potential enhancements for specific kinematic configurations, particularly when particles move perpendicularly to the field. These findings underscore the importance of incorporating non-perturbative field effects for accurate predictions relevant to ALP searches in astrophysical environments and terrestrial experiments utilizing strong magnets. The computed vertex tensor provides the necessary theoretical input for refining signal predictions and potentially guiding experimental search strategies.

8 Acknowledgements

I would like to thank my supervisor, Prof. Barbara Jäger, for her invaluable insights and support during our regular meetings. I am also grateful to Jose Medina for kindly answering some of my questions.

References

- [1] F. Zwicky. Die rotverschiebung von extragalaktischen nebeln. *Helvetica Physica Acta*, 6:110–127, 1933.
- [2] V.C. Rubin, W.K. Ford, Jr., and N. Thonnard. Rotational properties of 21 SC galaxies with a large range of luminosities and radii, from NGC 4605 (R=4kpc) to UGC 2885 (R=122kpc). 238:471–487, June 1980.
- [3] Richard Massey, Thomas Kitching, and Johan Richard. The dark matter of gravitational lensing. *Reports on Progress in Physics*, 73(8):086901, jul 2010.
- [4] Dhananjay Saikumar. Exploring the frontiers: Challenges and theories beyond the standard model, 2024.
- [5] Gerard Jungman, Marc Kamionkowski, and Kim Griest. Supersymmetric dark matter. *Physics Reports*, 267:195–373, 06 1995.
- [6] Julia Gehrlein and Mathias Pierre. A testable hidden-sector model for Dark Matter and neutrino masses. *JHEP*, 02:068, 2020.
- [7] Pavel Fileviez Pérez, Clara Murgui, and Alexis D. Plascencia. Neutrino-dark matter connections in gauge theories. *Phys. Rev. D*, 100:035041, Aug 2019.
- [8] Roberto D. Peccei. *The Strong CP Problem and Axions*, pages 3–17. Springer Berlin Heidelberg, Berlin, Heidelberg, 2008.
- [9] Asimina Arvanitaki, Savas Dimopoulos, Sergei Dubovsky, Nemanja Kaloper, and John March-Russell. String axiverse. *Phys. Rev. D*, 81:123530, Jun 2010.
- [10] H. Primakoff. Photo-production of neutral mesons in nuclear electric fields and the mean life of the neutral meson. *Phys. Rev.*, 81:899–899, Mar 1951.
- [11] Jean-François Fortin and Kuver Sinha. Constraining axion-like-particles with hard x-ray emission from magnetars. *Journal of High Energy Physics*, 2018(6), June 2018.
- [12] Jean-François Fortin, Huai-Ke Guo, Steven P. Harris, Doojin Kim, Kuver Sinha, and Chen Sun. Axions: From magnetars and neutron star mergers to beam dumps and becs. *International Journal of Modern Physics D*, 30(07):2130002, May 2021.
- [13] J. K. Vogel et. al. Iaxo - the international axion observatory, 2013.
- [14] S Andriamonje, S Aune, D Autiero, K Barth, A Belov, B Beltrán, H Bräuninger, JM Carmona, S Cebrián, JI Collar, et al. An improved limit on the axion–photon coupling from the cast experiment. *Journal of Cosmology and Astroparticle Physics*, 2007(04):010, 2007.
- [15] Allen Caldwell, Gia Dvali, Béla Majorovits, Alexander Millar, Georg Raffelt, Javier Redondo, Olaf Reimann, Frank Simon, and Frank Steffen. Dielectric haloscopes: A new way to detect axion dark matter. *Phys. Rev. Lett.*, 118:091801, Mar 2017.

- [16] T. Braine et al. Extended search for the invisible axion with the axion dark matter experiment. *Phys. Rev. Lett.*, 124:101303, Mar 2020.
- [17] N. Du et al. Search for invisible axion dark matter with the axion dark matter experiment. *Phys. Rev. Lett.*, 120:151301, Apr 2018.
- [18] P. Sikivie. Experimental tests of the "invisible" axion. *Phys. Rev. Lett.*, 51:1415–1417, Oct 1983.
- [19] Georg Raffelt and Leo Stodolsky. Mixing of the photon with low-mass particles. *Phys. Rev. D*, 37:1237–1249, Mar 1988.
- [20] Cédric Deffayet, Diego Harari, Jean-Philippe Uzan, and Matias Zaldarriaga. Dimming of supernovae by photon-pseudoscalar conversion and the intergalactic plasma. *Phys. Rev. D*, 66:043517, Aug 2002.
- [21] W. H. Furry. On bound states and scattering in positron theory. *Phys. Rev.*, 81:115–124, Jan 1951.
- [22] Julian Schwinger. On gauge invariance and vacuum polarization. *Phys. Rev.*, 82:664–679, Jun 1951.
- [23] A. A. Belavin, A. M. Polyakov, A. S. Schwartz, and Yu S. Tyupkin. Pseudoparticle solutions of the yang-mills equations. *Physics Letters B*, 59(1):85–87, October 1975.
- [24] Abel C. et al. Measurement of the permanent electric dipole moment of the neutron. *Phys. Rev. Lett.*, 124:081803, Feb 2020.
- [25] R. D. Peccei and Helen R. Quinn. CP conservation in the presence of pseudoparticles. 38(25):1440–1443, June 1977.
- [26] Gerard 't Hooft, C. Itzykson, A. Jaffe, H. Lehmann, P. K. Mitter, I. M. Singer, and R. Stora, editors. *Recent Developments in Gauge Theories. Proceedings, Nato Advanced Study Institute, Cargese, France, August 26 - September 8, 1979*, volume 59, 1980.
- [27] Stephen L. Adler. Axial-vector vertex in spinor electrodynamics. *Phys. Rev.*, 177:2426–2438, Jan 1969.
- [28] Jihn E. Kim. Weak-interaction singlet and strong CP invariance. *Phys. Rev. Lett.*, 43:103–107, Jul 1979.
- [29] M.A. Shifman, A.I. Vainshtein, and V.I. Zakharov. Can confinement ensure natural cp invariance of strong interactions? *Nuclear Physics B*, 166(3):493–506, 1980.
- [30] Michael Dine, Willy Fischler, and Mark Srednicki. A simple solution to the strong cp problem with a harmless axion. *Physics Letters B*, 104(3):199–202, 1981.
- [31] A P Zhitnitskii. Possible suppression of axion-hadron interactions. *Sov. J. Nucl. Phys. (Engl. Transl.); (United States)*, 31:2, 2 1980.

- [32] Giovanni Grilli Di Cortona, Edward Hardy, Javier Pardo Vega, and Giovanni Villadoro. The qcd axion, precisely. *Journal of High Energy Physics*, 2016(1):1–37, 2016.
- [33] Koichi Hamaguchi, Natsumi Nagata, Keisuke Yanagi, and Jiaming Zheng. Limit on the axion decay constant from the cooling neutron star in cassiopeia a. *Phys. Rev. D*, 98:103015, Nov 2018.
- [34] Steen Hannestad, Alessandro Mirizzi, and Georg Raffelt. New cosmological mass limit on thermal relic axions. *JCAP*, 07:002, 2005.
- [35] Masahiro Kawasaki, Eisuke Sonomoto, and Tsutomu T. Yanagida. Cosmologically allowed regions for the axion decay constant f_a . *Physics Letters B*, 782:181–184, 2018.
- [36] Howard Georgi, David B Kaplan, and Lisa Randall. Manifesting the invisible axion at low energies. *Physics Letters B*, 169(1):73–78, 1986.
- [37] Koichi Hattori, Kazunori Itakura, and Sho Ozaki. Strong-field physics in qed and qcd: From fundamentals to applications. *Progress in Particle and Nuclear Physics*, 133:104068, November 2023.
- [38] Claude Itzykson and Jean-Bernard Zuber. *Quantum field theory*. Courier Corporation, 2006.
- [39] VO Papanjan and VI Ritus. Vacuum polarization and photon splitting in an intense field. Technical report, CM-P00062608, 1971.
- [40] VO Papanyan and VI Ritus. The three-photon interaction in intense fields and scale invariance. *Zh. Eksp. Teor. Fiz*, 65:1756–1771, 1973.
- [41] Jorge Jaber-Urquiza and Angel Sanchez. Interaction field strength between a scalar particle and two massless vector bosons in the presence of an external magnetic field. *Phys. Rev. D*, 107:116024, Jun 2023.
- [42] Alejandro Ayala, Santiago Bernal-Langarica, Jorge Jaber-Urquiza, and José Jorge Medina-Serna. Two-gluon one-photon vertex in a magnetic field and its explicit one-loop approximation in the intermediate field strength regime. *Physical Review D*, 110(7), October 2024.
- [43] Vladyslav Shtabovenko, Rolf Mertig, and Frederik Orellana. FeynCalc 9.3: New features and improvements. *Comput. Phys. Commun.*, 256:107478, 2020.
- [44] Hurley K. et al. An exceptionally bright flare from sgr 1806–20 and the origins of short-duration gamma-ray bursts. *Nature*, 434(7037):1098–1103, April 2005.
- [45] Peter Svrcek and Edward Witten. Axions in string theory. *Journal of High Energy Physics*, 2006(06):051–051, June 2006.
- [46] G Peter Lepage. A new algorithm for adaptive multidimensional integration. *Journal of Computational Physics*, 27(2):192–203, 1978.